

# Experimental Research and Phase-field Simulation of Coarsening Kinetics of $\gamma$ Precipitates in Co-Ti Alloys

Wang Cuiping<sup>1</sup>, Huang Jianhong<sup>1</sup>, Lu Yong<sup>1</sup>, Liu Xingjun<sup>1,2</sup>

<sup>1</sup>Fujian Provincial Key Laboratory of Materials Genome, Xiamen University, Xiamen 361005, China; <sup>2</sup>Harbin Institute of Technology, Shenzhen 518055, China

**Abstract:** The microstructure evolution and coarsening behaviors of disordered  $\gamma$  phase in the inverse Co-19.7Ti alloy have been investigated by experiments and a phase-field method. Both the experimental and simulated results show that the morphologies of  $\gamma$  phase evolve from near-spherical shape to plate-like shape as the aging time increases. The coarsening kinetics for the mean particle size obeys the cube law  $r^3 = kt$ , and it can be obtained as:  $\bar{r}_t^3 = 1.126 \times 10^{19} t \exp[-349890/RT]$ . There exist two distinct stages of the mean particle size increase versus aging time, the growth rate is dramatically larger in the stage I and has a relatively slower increase in the stage II. The summit of precipitate size distributions becomes larger and the breadth of the distributions decreases from 700 °C to 750 °C. The simulated results reproduce well the experimental results.

**Key words:** Co-19.7Ti alloy; phase-field method; coarsening kinetics; temperature

The Co-based superalloys have attracted much attention of many researchers due to the discovery of the new L1<sub>2</sub> ordered strengthening  $\gamma'$  phase, that is Co<sub>3</sub>(Al,W), which precipitates from the disordered  $\gamma$  matrix in the Co-Al-W system<sup>[1]</sup>. Up to now, various efforts have been made to the alloying of Co-Al-W based alloys, in order to improve its strength and  $\gamma'$  solvus temperature<sup>[2-4]</sup>. It is believed that Co-based superalloys may have the possibility to replace Ni-based superalloys to be utilized at high temperature environment.

Nevertheless, Kobayashi et al.<sup>[5]</sup> noted that the Co<sub>3</sub>(Al,W) phase is metastable. The mechanical properties of alloys will be reduced due to the low thermodynamic stability of  $\gamma'$  phase at high temperatures. For the Co-Ti binary system, there exists a stable  $\gamma'$ -Co<sub>3</sub>Ti phase. Moreover, Co-Ti alloys have a good resistance to corrosion and positive temperature dependence of flow stress<sup>[6]</sup>. Nonetheless, the applications of the Co-Ti alloys are restricted due to the low melting temperature and the large misfit between  $\gamma$  and  $\gamma'$  phases<sup>[7, 8]</sup>. Recently, in pursuance of improving the strength, ductility and creep resistance of Co-Ti alloys, the ductile  $\gamma$  phase precipitated from  $\gamma'$  phase

has been introduced by researchers<sup>[9, 10]</sup>. Takesue et al.<sup>[10]</sup> reported that the creep strength of Co-Ti alloys increased owing to the precipitation of disordered  $\gamma$  phase. It is well known that the properties of the alloys are greatly dependent upon the morphology, size and coarsening behaviors of the precipitates. The coarsening behaviors of disordered  $\gamma$  phase in inverse Ni-Al alloys have been studied in recent years<sup>[11, 12]</sup>. However, there are few reports of the coarsening behaviors of disordered  $\gamma$  phase in inverse Co-Ti alloys available in the literature.

The understanding of microstructure evolution during the aging process is necessary to improve the heat treatment process. The phase-field method is served to predict the complex microstructure evolution, and its practical applications are successful in various materials. To date, numerous researchers have studied the microstructure evolution of the precipitates by phase field simulation in Ni-based superalloys<sup>[13-17]</sup>. Consequently, this paper aims to combine the experiment and phase field method to investigate the coarsening behaviors of  $\gamma$  phase in inverse Co-Ti alloys.

Received date: May 18, 2018

Foundation item: National Key R&D Program of China (2017YFB0702901, 2016YFB0701401); Ministry of Science and Technology of China (2014DFA53040); Fundamental Research Funds for the Central Universities (20720180072)

Corresponding author: Liu Xingjun, Professor, Department of Materials Science and Engineering, College of Materials, Xiamen University, Xiamen 361005, P. R. China, Tel: 0086-592-2187888, E-mail: lxj@xmu.edu.cn

Copyright © 2019, Northwest Institute for Nonferrous Metal Research. Published by Science Press. All rights reserved.

## 1 Methodology

### 1.1 Experimental methods

In this work, the Co-19.7Ti alloy (nominal composition) was selected to investigate the microstructure. Because the mass losses of the alloy were less than 0.1%, this work considered the alloy composition equal to the nominal composition. The cast Co-19.7Ti alloy was enclosed in a quartz tube, which was filled with argon. Then it was put into a vacuum furnace at 1150 °C for 24 h to obtain the homogenized samples. Subsequently, the homogenized samples were put into the vacuum furnace at 700, 750 and 800 °C for different times and then quenched into icy water. The samples were treated by standard metallographic techniques and then etched in a solution of HCl (75vol%) + HNO<sub>3</sub> (25vol%) for 5~10 s at room temperature. Scanning electron microscope (SEM) was used to investigate the microstructure of Co-19.7Ti alloy. The IMAGE Je software was used to measure the volume fraction and the size of the  $\gamma$  precipitates.

### 1.2 Simulation model

In this work, the concentration profile is characterized by using the composition field. The phase transformation is described by using three order parameter fields. The temporal evolution of the composition field and order parameter fields is obtainable by the Cahn-Hilliard diffusion equation and the Ginzburg-Landau equation, respectively<sup>[18]</sup>:

$$\frac{\partial c}{\partial t} = M \nabla^2 \frac{\delta F}{\delta c} + \xi_c \quad (1)$$

$$\frac{\partial \eta_i}{\partial t} = -L \frac{\delta F}{\delta \eta_i} + \xi_i \quad i = 1, 2, 3 \quad (2)$$

where  $c$  is the composition,  $\eta_i$  is the order parameter,  $L$  and  $F$  are the structural relaxation and the total free energy, respectively, and  $M$  is diffusion mobilities, as  $M = c_0(1-c_0)D/RT$ <sup>[13]</sup>.  $\xi_c$  and  $\xi_i$  are the random noise terms, which are mainly for nucleation.

#### 1.2.1 Free energy

Taking into consideration the coherent precipitation, the total free energy can be expressed as  $F = F_c + F_{el}$ , where  $F_c$  is chemical free energy, and  $F_{el}$  is the elastic strain energy.

The chemical free energy of the  $\gamma$  ( $\alpha$ Co) phase in the Co-Ti alloys can be characterized as follows:

$$F_{Co} = \sum_{i=Co,Ti} c_i G_i + RT \sum_{i=Co,Ti} c_i \ln c_i + {}^{ex}G + {}^{mag}G \quad (3)$$

where  $c_i$  is the mole concentration of Co or Ti,  $G_i$  is the molar free energy of Co or Ti,  ${}^{ex}G$  is the excess energy and  ${}^{mag}G$  is magnetic free energy. The thermodynamic data in Eqs.(3) are obtained from the Co-Ti thermodynamic database<sup>[8]</sup>.

Consequently, the chemical free energy of the  $\gamma$  ( $\alpha$ Co) phase at  $T=700$  °C is obtained as follows:

$$\begin{aligned} F_{\gamma(c_{Ti})} = & 489000c_{Ti}^4 - 233400c_{Ti}^3 + 87156.2c_{Ti}^2 + \\ & c_{Ti}(-67780.23 + 8089.522 \ln(c_{Ti})) - 8089.522 \\ & \ln(1 - c_{Ti}) + 8089.522 \ln(1 - c_{Ti}) - 42688 \end{aligned} \quad (4)$$

The chemical free energy of  $\gamma'$  phase in Co-Ti alloys at 700 °C can be simplified by an eight-order polynomial:

$$\begin{aligned} F_{\gamma'(c_{Ti})} = & -6831000000c_{Ti}^8 + 8389000000c_{Ti}^7 - \\ & 4056000000c_{Ti}^6 + 981700000c_{Ti}^5 - 119300000c_{Ti}^4 \\ & + 5082000c_{Ti}^3 + 238200c_{Ti}^2 - 109700c_{Ti} - 42700 \end{aligned} \quad (5)$$

The comparison of the Gibbs energy obtained from the Eqs. (4) and Eqs. (5) with that obtained by the Pandat calculation in Co-Ti alloys at 700 °C is shown in Fig.1. This indicates that the free energy curve in this work agrees well with that of the Pandat calculation. The same method is used to deal with chemical free energy at 750 °C.

In order to connect the free energy of the two-phase through the structural order parameters, an interpolation function  $H(\eta_i) = \eta_i^3(10 - 15\eta_i + 6\eta_i^2)$  is used in this work, which satisfies  $H(0)=0$ ,  $H(1)=1$ , and  $dH/d\eta|_{\eta=0} = dH/d\eta|_{\eta=1} = 0$ <sup>[19]</sup>. Because the  $\gamma$  phase has the disordered fcc structure, the order parameters are equivalent, e.g.  $\eta = \eta_1 = \eta_2 = \eta_3$ . Thus, the bulk chemical free energy density can be expressed as:

$$f(c_{Ti}, \eta) = V_m^{-1} [(1 - H(\eta))F_{\gamma(c_{Ti})} + H(\eta)F_{\gamma'(c_{Ti})}] \quad (6)$$

where  $V_m$  is molar volume,  $V_m = 5.42 \times 10^{-5} \text{ m}^3 \cdot \text{mol}^{-1}$  in this work.

Including the gradient energy terms, the chemical free energy of the system could be expressed as follows<sup>[20]</sup>:

$$F_{ch} = \int_V \left[ f(c_{Ti}, \eta) + \frac{1}{2} k_\eta (\nabla \eta)^2 + \frac{1}{2} k_c (\nabla c)^2 \right] dV \quad (7)$$

where  $k_c$  and  $k_\eta$  are the gradient energy coefficients for concentration and order parameter fields.

Khachatryan's model is used to describe the elastic strain energy, which can be expressed as<sup>[21]</sup>:

$$F_{el} = \frac{1}{2} \int B(\mathbf{n}) |\tilde{c}(\mathbf{k})|^2 \frac{d^3 k}{(2\pi)^3} \quad (8)$$

where  $\tilde{c}(\mathbf{k})$  is the Fourier transform of  $c(\mathbf{r})$  and  $\mathbf{k}$  is the wave vector,  $\mathbf{n} = \mathbf{k}/k$  is a unit vector in reciprocal space.

For the 2-D case,  $B(\mathbf{n})$  can be approximated as follows<sup>[22]</sup>:

$$B(\mathbf{n}) \approx B_{el} \varepsilon_0^2 n_x^2 n_y^2 \quad (9)$$

where  $\varepsilon_0$  is an arbitrary stress-free transformation strain.  $n_x$  and  $n_y$  are the components of  $\mathbf{n}$  along the  $x$ -axis and  $y$ -axis in the reciprocal space.  $B_{el}$  is a material constant to describe the elastic properties, and is expressed as:

$$B_{el} = \frac{-4\zeta(C_{11} + 2C_{12})^2}{C_{11}(C_{11} + C_{12} + 2C_{44})} \quad (10)$$

$\zeta = C_{11} - C_{12} - 2C_{44}$  is a constant to describe the elastic anisotropy of the system.  $C_{11}$ ,  $C_{12}$  and  $C_{44}$  are the elastic constants.

#### 1.2.2 Dimensionless phase-field kinetic equations

A reduced time  $t^*$  and reduced spatial coordinates  $r^*$  have been introduced to transform Eq.(1) and Eq.(2) into a dimensionless form. The  $t^*$  and  $r^*$  are given by  $t^* = Lt|\Delta f|V_m$  and  $r^* = r/l$ . In this work,  $|\Delta f| = 1.07 \times 10^8 \text{ J} \cdot \text{m}^{-3}$  is used to normalize the Gibbs free energy, and  $l = 2.87 \times 10^{-9} \text{ m}$  is the length

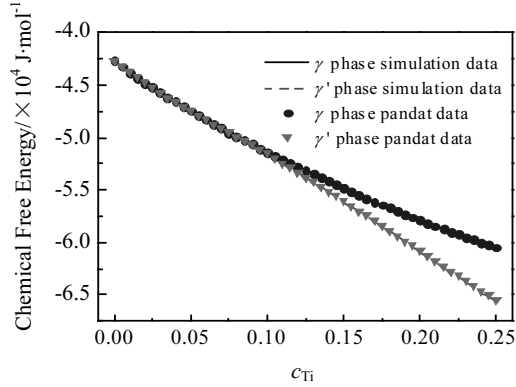


Fig.1 Comparison of chemical free energy obtained in this work with that obtained by the pandat calculation at 700 °C

unit in the simulation<sup>[14]</sup>. The dimensionless form is shown as follows:

$$\frac{\partial c(\mathbf{r}^*, t^*)}{\partial t^*} = \chi(\nabla^*)^2 \left[ \frac{\delta f^*}{\delta c(\mathbf{r}^*, t^*)} - k_c^*(\nabla^*)^2 c(\mathbf{r}^*, t^*) + \frac{\delta F_{el}^*}{\delta c(\mathbf{r}^*, t^*)} \right] + \xi_c^*(\mathbf{r}^*, t^*) \quad (11)$$

$$\frac{\partial \eta_i(\mathbf{r}^*, t^*)}{\partial t^*} = - \left[ \frac{\delta f^*}{\delta \eta_i(\mathbf{r}^*, t^*)} - k_\eta^*(\nabla^*)^2 \eta_i(\mathbf{r}^*, t^*) \right] + \xi_{\eta_i}^*(\mathbf{r}^*, t^*) \quad i = 1, 2, 3 \quad (12)$$

where  $\chi = M/Ll^2$ ,  $k_c^* = k_c/|\Delta f|^2$ ,  $k_\eta^* = k_\eta/|\Delta f|^2$ ,  $F_{el}^* = F_{el}/|\Delta f|$ .  $k_c = 7.05 \times 10^{-9} \text{ J}\cdot\text{m}^{-1}$ ,  $k_\eta = 1.23 \times 10^{-10} \text{ J}\cdot\text{m}^{-1}$ . Similar to the variation of diffusion mobilities  $M$  with temperature, this work assumes  $\chi$  as a function of temperature following an exponential law  $\chi(T) = \chi_0 \cdot c_0(1-c_0)\exp(-Q/RT)/RT$ . To get a reasonable microstructure, this work employs a fixed value  $1.32c_0(1-c_0)$  for  $\chi$  at 700 °C in the Co-Ti system, and  $L = 4.31 \times 10^{-8} \text{ mol}\cdot\text{J}^{-1}\cdot\text{s}^{-1}$  guarantees a diffusion-controlled process. The  $Q$  used in this work is  $349.89 \text{ kJ}\cdot\text{mol}^{-1}$ . As a result,  $\chi_0$  is determined to be  $6.49 \times 10^{22}$ , and  $\chi$  can be given by  $\chi(T) = [6.49 \times 10^{22} c_0(1-c_0)\exp(-3.4989 \times 10^5/RT)]/RT$ . The lattice misfit  $\delta = 1.67\%$  at 700 °C and  $\delta = 1.36\%$  at 800 °C<sup>[7]</sup>. In this work, we suppose the  $\delta$  is linearly related to temperature between  $T = 700 \text{ °C}$  and  $T = 800 \text{ °C}$ . Therefore,  $\delta = 1.51\%$  can be obtained at  $T = 750 \text{ °C}$ . The parameters  $\varepsilon_0$  can be estimated by  $\varepsilon_0 = \delta/(c_\gamma - c_\gamma)$ . The elastic constants for Co-Ti system are  $C_{11} = 2.686 \times 10^{11} \text{ J}\cdot\text{m}^{-3}$ ,  $C_{12} = 1.678 \times 10^{11} \text{ J}\cdot\text{m}^{-3}$ ,  $C_{44} = 1.186 \times 10^{11} \text{ J}\cdot\text{m}^{-3}$ <sup>[23]</sup>.

## 2 Results and Discussion

### 2.1 Experimental observations

#### 2.1.1 Morphology and evolution

The microstructure evolution of  $\gamma$  precipitates in Co-19.7Ti alloy, aged at 700, 750 and 800 °C for different times is shown in Fig.2. According to Fig.2a~Fig.2j, it can be seen that the morphology of the  $\gamma$  phase is near-spherical in the early period

of aging, and grows from near-spherical to plate-like shape as the aging time increases. For long aging time, such as in Fig.2c, 2f and 2j, many plate-like precipitates are obvious. Fig.2g shows that spatial correlations do not exist in the early period of aging, but in alignment evidently at long aging time. As the temperature increases, the  $\gamma$  precipitates coarsen apparently. Unlike the microstructure evolution of  $\gamma$  precipitates in Ni-Al alloys, almost none are equiaxed in shape after 48 h in Co-19.7Ti alloy<sup>[11, 12]</sup>.

#### 2.1.2 Coarsening kinetics of $\gamma$ particles

The mean size of the  $\gamma$  precipitates in Co-19.7Ti alloy can be obtained by<sup>[16]</sup>

$$r = \sqrt{V_f / \pi N(t)} \quad (13)$$

where  $V_f$  and  $N(t)$  are the volume fraction and the particle number of  $\gamma$  precipitates, respectively. The mean size of  $\gamma$  precipitates with different aging time at 700, 750 and 800 °C is listed in Table 1. It can be seen that the larger size of  $\gamma$  precipitates can be acquired with higher temperature. Fig.3a shows the mean size of  $\gamma$  precipitates plotted as  $r^3$  versus  $t$ . Apparently, the growth of particles in Co-Ti alloys follows the linear relationship,  $r^3 = kt$ , where  $k$  is the coarsening rate constant. The relationship illustrates that the coalescence of  $\gamma$  particles in the  $\gamma'$  phase obeys the diffusion-controlled growth behavior. Therefore,  $k$  can be calculated, as 1.89, 14.03 and  $107.95 \text{ nm}^3/\text{min}$  at 700, 750 and 800 °C, respectively.

The coarsening kinetics in superalloys can be described well on the basis of the classical Lifshitz-Slyozov-Wagner (LSW) theory<sup>[24, 25]</sup>. Accordingly, the  $k$  can be formulated as follows:

$$k = \frac{8D\sigma C_e V_m^2}{9RT} \quad (14)$$

where  $D = D_0 \exp(-Q/RT)$  is the temperature-dependent diffusion coefficient of the rate controlling solute in the matrix,  $Q$  is the activation energy for  $\gamma$  particles coarsening,  $C_e$  is the equilibrium concentration of the solute in the matrix,  $\sigma$  is the matrix/precipitate interfacial energy, and  $V_m$  is the molar volume of the precipitate. Considering these experimentally determined parameters, Eq.(15) can be written as follows:

$$\ln \left( k \frac{T}{C_e} \right) = \text{constan } t - \frac{Q}{RT} \quad (15)$$

Table 1 Comparison of the mean size of  $\gamma$  precipitates with aging time when aging at 700, 750 and 800 °C

Aging time/h	Mean size/nm		
	700 °C	750 °C	800 °C
8	-	-	39.05
24	-	-	55.12
48	12.28	32.94	70.06
196	24.07	55.51	105.22
480	35.64	73.78	146.36
750	43.23	-	-

$T/C_e$  can be ignored in this work because it has no significant change from 700 °C to 800 °C<sup>[26]</sup>. Fig.3b shows the  $\ln k$  as a function of  $T^{-1}$ . The expression  $\ln k=43.868-42085.164/T$  can be obtained from the fitted line in Fig.3b. The value of  $Q$  is gained to be 349.89 kJ·mol<sup>-1</sup> for Co-Ti alloys. The coarsening rate constant  $k$  of  $\gamma$  precipitates is calculated by  $k = e^{43.868} \exp(-349890/RT)$  according to the expression obtained in Fig.3b. Consequently, the linear relationship, which is related to the coarsening of  $\gamma$  particles, can be expressed as  $\bar{r}_t^3 = 1.126 \times 10^{19} t \exp[-349890/RT]$ , where  $t$  is aging time. This expression can be used to predict the change of  $\gamma$  precipitates size in the process of aging.

## 2.2 Simulation results and discussion

The simulation domain has a square form with a domain size of 512×512 cells for Co-19.7Ti alloy at 700 and 750 °C. The dimensionless time step and grid spacing used in the simulation are set as  $\Delta t^* = 1.0 \times 10^{-4}$  and  $\Delta x^* = \Delta y^* = 1$ , respectively.

### 2.2.1 Morphology evolution of $\gamma$ particles

The morphology evolution of  $\gamma$  phase starting from nucleation is simulated for the Co-19.7Ti alloy at 700 and 750 °C, as shown in Fig.4. Fig.4a<sub>1</sub>~a<sub>4</sub> shows that the morphology of  $\gamma$  phase is nearly spherical in shape at the initial stage, rectangle and plate-shaped particles merge regularly along the elastically soft [10] or [01] directions as the aging time increases. By comparing Fig.4a with Fig.4b, quite evidently, the mor-

phology of  $\gamma$  phase changes significantly with increasing temperature. The morphology evolution indicates that the interfacial energy is dominant when the particle size is small at the initial stage, and the elastic energy begins to play a dominant role when the particle size becomes larger as the aging time increases. The growth and coalescence of the  $\gamma$  phase are through two mechanisms, such as the  $\gamma$  particles inside the ellipse A and B growing into the ellipse A\* and B\*, as demonstrated in Fig.4a<sub>2</sub> and a<sub>3</sub>. The specific evolution of coarsening of  $\gamma$  particles is presented in Fig.4c and 4d. The former process is related to the merging of particles on each other to form larger particles. The later form is connected with the atomic exchange between the  $\gamma$  precipitates by means of the diffusion through the  $\gamma'$  matrix, which causes the smaller particles dwindling gradually and larger particles growing. Compared with the experimental results shown in Fig. 2, it is clear that the simulation results agree well with the experimental observation.

### 2.2.2 Composition evolution of $\gamma$ particles

Fig.5 demonstrates the composition evolution of  $\gamma$  phase for Co-19.7Ti alloy at different temperatures. The  $\gamma$  phase composition decreases with the increase of aging time, and then reaches the equilibrium value  $c_{Ti}=0.048$  and 0.042, where the equilibrium value shows little deviation from the Co-Ti thermodynamic phase diagram ( $\sim 0.039$  and 0.033) at 750 and 700 °C, respectively<sup>[8]</sup>. The time, when the composition reaches

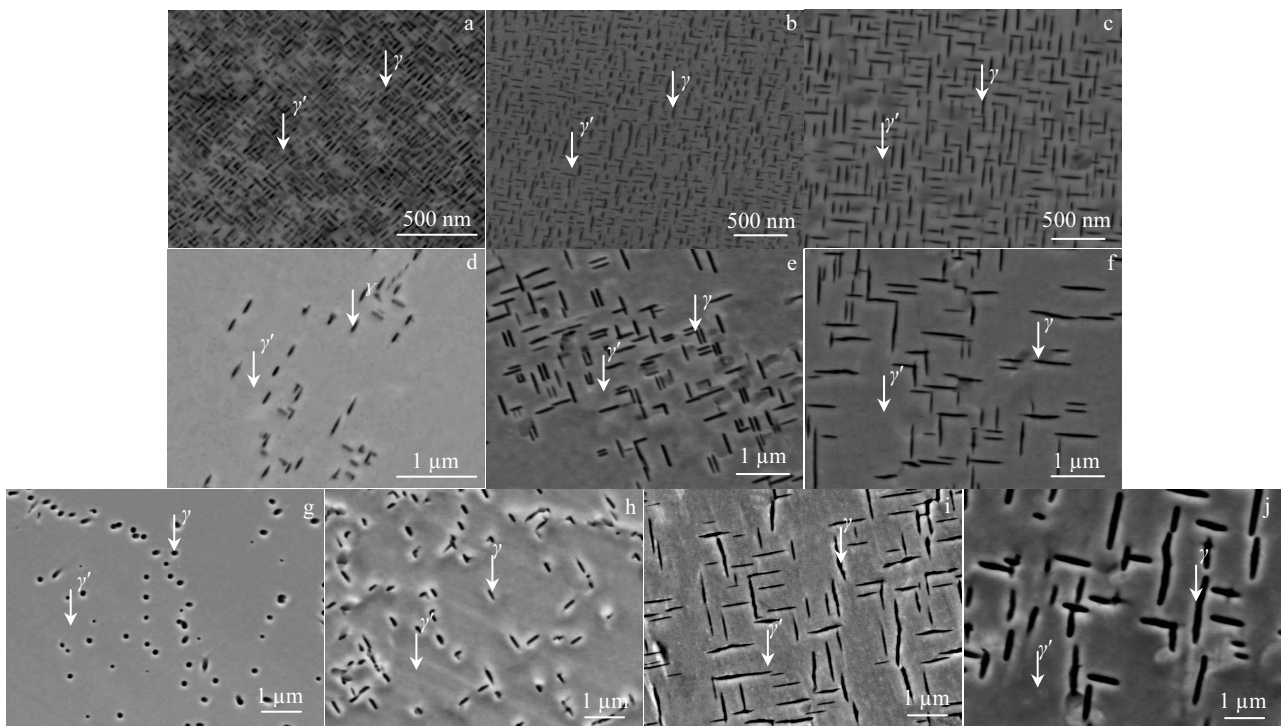


Fig.2 SEM micrographs of  $\gamma$  precipitates in Co-19.7Ti alloy aged at 700 °C for 48 h (a), 196 h (b), 480 h (c); aged at 750 °C for 48 h (d), 196 h (e), 480 h (f); aged at 800 °C for 8 h (g), 24 h (h), 196 h (i), 480 h (j)

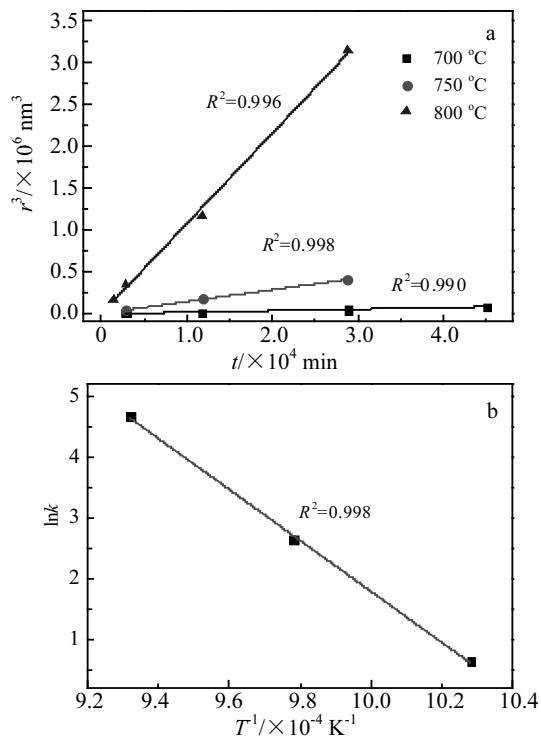


Fig.3 Cube of the mean particle sizes ( $r$ ) versus aging time for the Co-19.7Ti alloy aged at 700, 750 and 800 °C (a), and Arrhenius plots of the activation energy for  $\gamma$  particles coarsening (b)

the equilibrium value, is approximately 40 and 60 h at 750 and 700 °C, respectively. The results illustrate the increase of temperature causes the fast phase transformation. When  $t=480$  h, the distribution of Ti equilibrium content at 750 °C is wider than that at 700 °C. It indicates that the increasing temperature accelerates the coarsening of the  $\gamma$  precipitates.

### 2.2.3 Variation of volume fraction and particle number of $\gamma$ particles

Fig.6a shows the volume fraction of  $\gamma$  phase changes versus aging time in the Co-19.7Ti alloy at different aging temperatures, including experimental results, simulation results and the results obtained by the Co-Ti phase diagram<sup>[8]</sup>. The volume fraction of  $\gamma$  phase increases rapidly at the initial stage, then tends to be smooth and finally reaches stability as the aging time increases. This variation trend is similar to  $\gamma'$  phase<sup>[17]</sup>. The equilibrium volume fraction of  $\gamma$  phase is 0.165 and 0.134 at 700 and 750 °C, respectively, which is lower than that of the Co-Ti phase diagram<sup>[8]</sup>. However, the calculated results are close to the experimental results ( $\sim 0.171$  and  $0.129$ ). The precipitation of  $\gamma$  particles is suppressed because the elastic strain field induced by the large misfit between  $\gamma$  and  $\gamma'$  phases in Co-Ti alloys. The larger the misfit increment, the lower the last volume fraction can be obtained<sup>[27]</sup>.

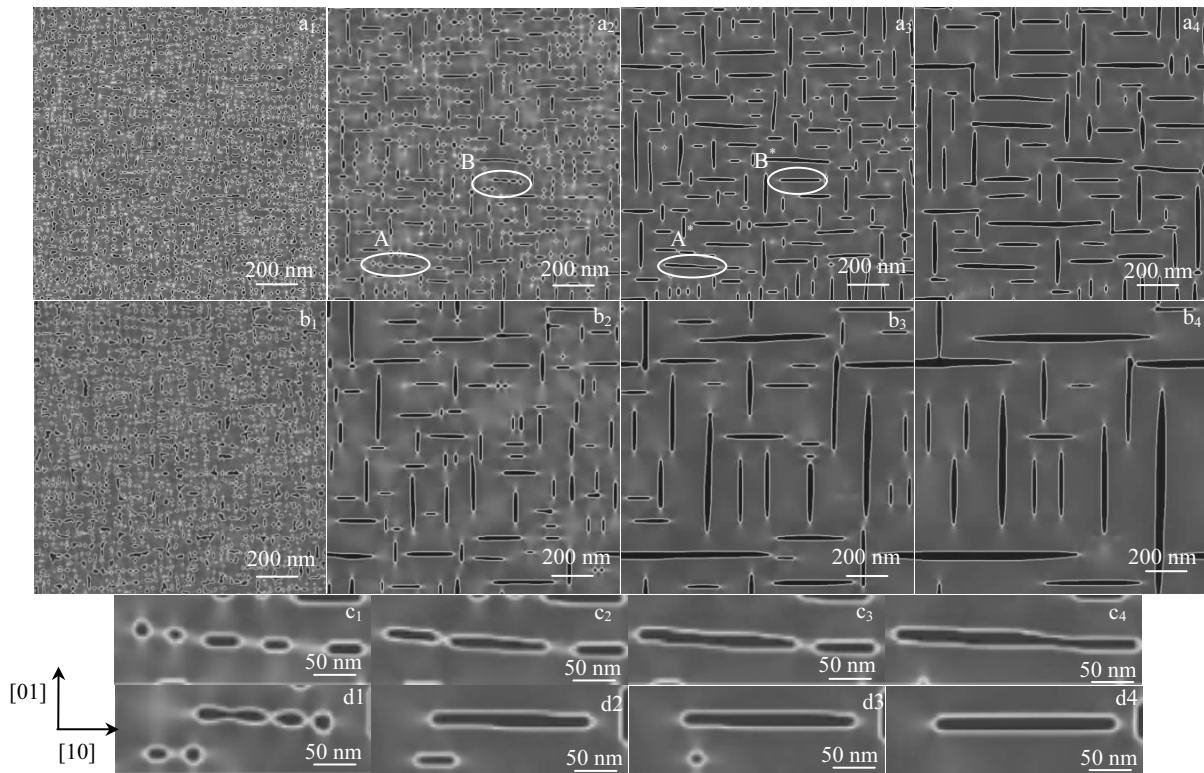


Fig.4 Morphologies evolution of  $\gamma$  precipitates in Co-19.7Ti alloy at different temperatures: (a)  $T=700$  °C, (b)  $T=750$  °C, (1-4)  $t=2, 48, 196, 480$  h; (c) the  $\gamma$  precipitates inside the ellipse A in Fig.4a<sub>2</sub> grow into the ellipse A\* in Fig.4a<sub>3</sub>; (d) the  $\gamma$  precipitates inside the ellipse B in Fig.4a<sub>2</sub> grow into the ellipse B\* in Fig.4a<sub>3</sub>, (1-4)  $t=48, 100, 150, 196$  h

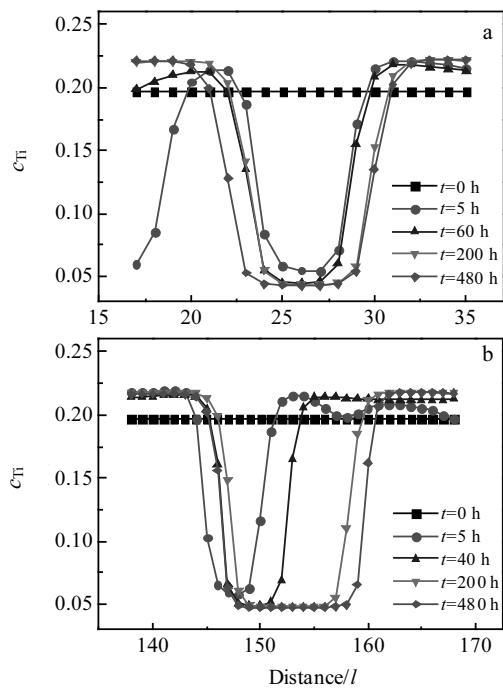


Fig.5 Composition evolution of  $\gamma$  phase in Co-19.7Ti alloy at different temperatures ( $l=2.87\times 10^{-9}$  m): (a)  $T=700$  °C and (b)  $T=750$  °C

Fig.6b reveals the particle number changes versus time in the Co-19.7Ti alloy at different aging temperatures. The number of particles increases rapidly as the aging time increases, then decreases sharply and finally reaches stability. The particles merge and decrease faster as the temperature rises.

#### 2.2.4 Variation of mean size of $\gamma$ particles

The evolution of the mean size of  $\gamma$  phase with increasing time in Co-19.7Ti alloy at different temperatures, as revealed in Fig.7a, including both the experimental and simulation results. The simulation results show that there are two distinct stages of the mean particle size of  $\gamma$  phase increase versus time. The growth rate of the mean particle size in the stage I is dramatically larger as a result of the growth of newly emerged particles from nucleation. Stage II has a relatively slower increase in mean particle size associated with the soft impingement of the diffusion field in the later growth and coarsening regimes. The division of the evolution of  $\gamma$  particle size is similar to the evolution of  $\gamma'$  particle size<sup>[17]</sup>.

The cube of the mean size  $\langle r \rangle^3$  versus  $t$  at different aging temperatures is shown in Fig.7b, with both the experimental and simulation results included. It can be seen that the data from the simulations can be well fitted to the cubic growth law, and  $k$  obtained from simulations is 1.85, and 13.76 nm<sup>3</sup>/min for aging at 700 and 750 °C, respectively. The comparison indicates that the simulation results are in good agreement with the experiments.

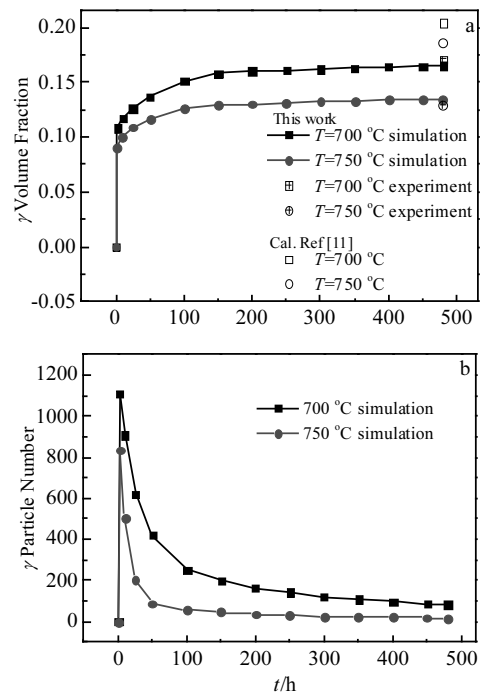


Fig.6 Evolution of volume fraction (a) and particle number (b) of  $\gamma$  precipitates versus time in Co-19.7Ti alloy at different temperatures

#### 2.2.5 Variation of mean aspect ratio of $\gamma$ particles

Aspect ratio is defined as the ratio of the long axis to the short axis of the  $\gamma$  particles. The dependence of mean aspect ratio on aging time for the Co-19.7Ti alloy at different temperatures is shown in Fig.8, as well as the experimental results. It is apparent that the mean aspect ratio also shows two stages with increasing aging time which is similar to the change of the mean size. The comparison reveals that the variation trends of the mean aspect ratio between simulations and experiments are very similar.

The mean aspect ratio of the  $\gamma$  phase in the Co-19.7Ti alloy largely outweighs that in the Ni-Al alloys<sup>[12]</sup>. Because the misfit between  $\gamma$  and  $\gamma'$  phases in Co-Ti system is larger than that in Ni-Al system. Accordingly, the larger elastic energy in Co-Ti system and the  $\gamma$  precipitates are unrestricted by the antiphase domains, which may cause the  $\gamma$  precipitates to merge more easily along the soft direction. Therefore, the microstructure of the  $\gamma$  phase in Co-19.7Ti alloy presents plate-like shape, while the  $\gamma$  phase in Ni-Al alloys exhibits square and rectangle shape at the same aging time.

#### 2.2.6 Particle size distributions of $\gamma$ phase

The particle size distributions of  $\gamma$  phase in the Co-19.7Ti alloy are shown in Fig.9, where the Y axis represents PSDs of  $\gamma$  phase, which is expressed as  $g(x)$ , and the  $x=r/\langle r \rangle$  represents the relative size of the particles, ( $r$  is the particle size,  $\langle r \rangle$  is the mean particle size). The PSDs were calculated as<sup>[15]</sup>:

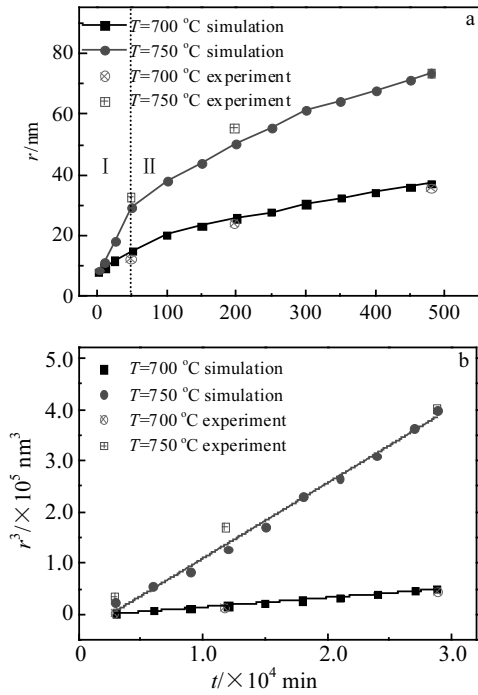


Fig.7 Evolution of mean size (a) and cube of size (b) of  $\gamma$  precipitates versus time in Co-19.7Ti alloy at different temperatures

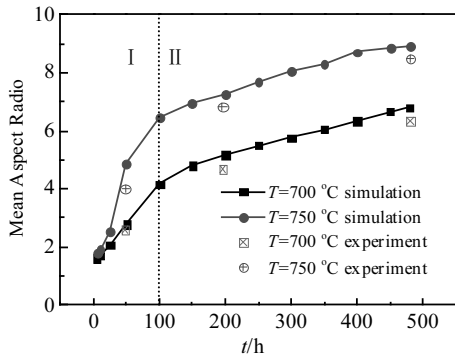


Fig.8 Comparison of the mean aspect ratio as a function of time obtained by simulations and experiments in Co-19.7Ti alloy at different temperatures

$$g(x) = \frac{N(x)x}{\Delta x N} \quad (16)$$

where  $N(x)$  is the number of particles in the range  $x \pm \Delta x / 2$  with  $\Delta x = 0.2$  and  $N$  is the total number of particles. The experiments (dots), simulations (histograms), and the LSW theory (dashed-dotted lines) are shown. Fig.9a~9d shows the PSDs of  $\gamma$  particles versus aging time in the Co-19.7Ti alloy at 700 °C. It can be seen that the summit of the PSDs falls gradually, the position of the PSDs summit shifts from 0.8 to 1.0 and the breadth of the distributions increases as the time

increases. Because the size of  $\gamma$  particles is small and similar at the initial stage, as shown in Fig.4a<sub>1</sub>. The growth and coarsening progresses of  $\gamma$  particles, as shown in Fig.4c and 4d, lead to the distributions of particles size broadened.

Fig.9e illustrates the PSDs of  $\gamma$  particles for  $t = 196$  h at 750 °C in the Co-19.7Ti alloy. Compared with Fig.9c, the summit of PSDs increases with the rise of aging temperature. In addition, the smaller precipitates disappear from experimental and simulated PSDs at 750 °C. This phenomenon is also found from Boisse et al<sup>[15]</sup>, the smaller precipitates disappear with decreasing  $\gamma$  phase volume fraction. According to Boisse et al, the growth and coarsening of the  $\gamma$  particles are dependent on the diffusional and elastic interactions between the particles if ordering is not considered in the kinetics. In this work, the  $\gamma$  phase volume fraction at 750 °C is lower than that at 700 °C and the diffusion rate of alloying elements at 750 °C is higher than that at 700 °C, which cause the small neighboring particles merge quickly in the stage I of coarsening.

In this work, the simulated PSDs do not agree with the PSDs predicted by the LSW theory, but fit well the PSDs of the experimental results. The PSDs of the experimental and simulation results are both with smaller summits which are shifted to the left side (smaller size) by comparison with the PSDs predicted by the LSW theory. Generally, the PSDs predicted by the LSW theory do not consider the effect of elastic energy and are only applicable for the case of the spherical shape precipitates with an infinitesimally small volume fraction. Nevertheless, in this work, the volume fraction of  $\gamma$  precipitates is large enough. Large elastic strain field is induced because the lattice misfit between  $\gamma$  and  $\gamma'$  phases in the Co-Ti system could not be ignored.

### 3 Conclusions

1) Both the experimental and simulated results show that the morphologies of  $\gamma$  phase in Co-19.7Ti alloy evolve from near-spherical to plate-like shape as the aging time increases.

2) As the temperature rises, the  $\gamma$  precipitates coarsen apparently. The coarsening kinetics for the mean particle size obeys the cube law  $r^3 = kt$ , and it can be obtained as:  $\bar{r}_t^3 = 1.126 \times 10^{19} t \exp[-349890/RT]$ . The coarsening rate constant  $k$  obtained from simulations is 1.85 and 13.76  $\text{nm}^3/\text{min}$  for 700 and 750 °C, respectively, which is close to the experimental results (1.89 and 14.03  $\text{nm}^3/\text{min}$ ).

3) Both the evolution of the mean particle size and mean aspect ratio have two distinct stages. The growth rate is dramatically larger in the stage I and has a relatively slower increase in the stage II. The summit of PSDs becomes smaller and the position of the PSDs summit shifts from 0.8 to 1.0 with the increase of aging time. The summit of PSDs becomes larger and the breadth of the distribution decreases from 700 to 750 °C at the same time. The simulation results fit well with the experimental results.

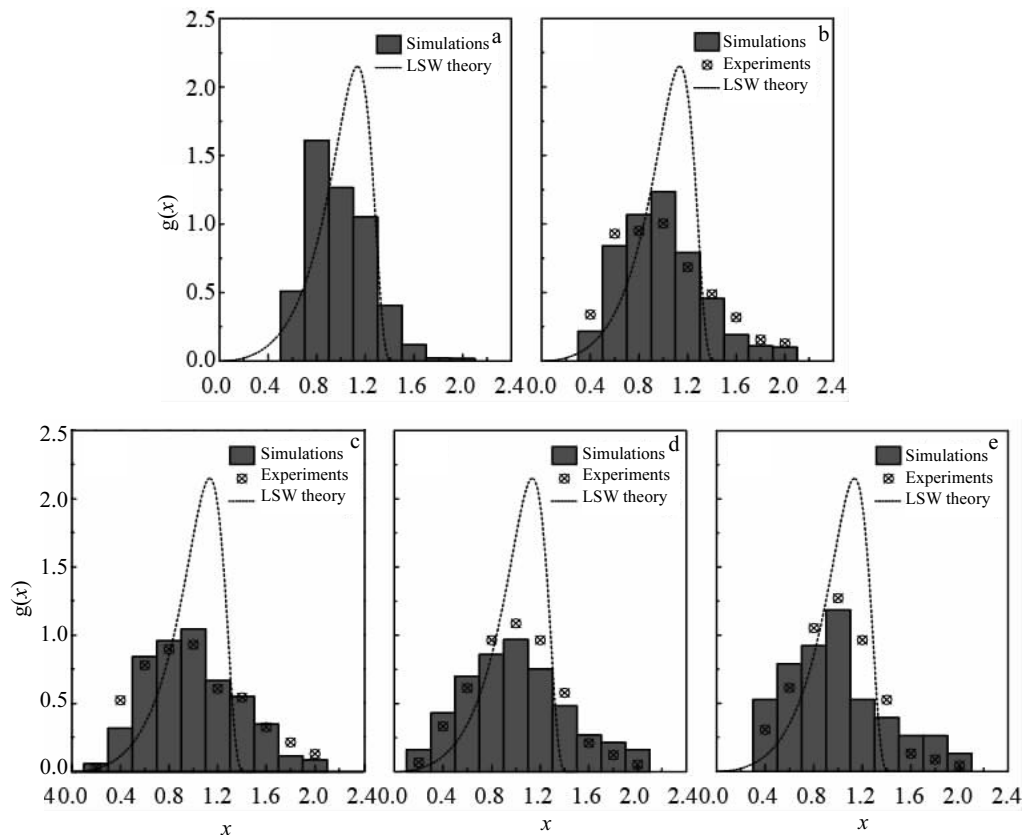


Fig.9 Comparison of the particle size distributions obtained by simulations, experiments and LSW theory in Co-19.7Ti alloy versus time (10 h, 48 h, 196 h and 480 h) at 700 °C (a-d), and 196 h at 750 °C (e)

## References

- Sato J, Omori T, Oikawa K et al. *Science*[J], 2006, 312(5770): 90
- Xue F, Mi T, Wang M et al. *Acta Metallurgica Sinica*[J], 2014, 50(7): 845 (in Chinese)
- Kobayashi S, Tsukamoto Y, Takasugi T. *Intermetallics*[J], 2012, 31: 94
- Povstugar I, Pa Choi P, Neumeier S et al. *Acta Materialia*[J], 2014, 78: 78
- Kobayashi S, Tsukamoto Y, Takasugi T et al. *Intermetallics*[J], 2009, 17(12): 1085
- Kim W Y, Hanada S, Takasuqi T. *Scripta Materialia*[J], 1997, 37(7): 1053
- Viatour P, Drapier J M, Coutsouradis D. *Cobalt*[J], 1973, 3: 67
- Davydov A, Kattner U, Josell D et al. *Metallurgical & Materials Transactions A*[J], 2001, 32(9): 2175
- Kaneno Y, Nakamura T, Inoue H et al. *Acta Materialia*[J], 2003, 51(7): 2113
- Takesue H, Ohishi K, Horita Z et al. *Materials Science & Engineering A*[J], 1997, 239-240(1): 479
- Ma Y, Ardell A. *Scripta Materialia*[J], 2005, 52(12): 1335
- Ma Y, Ardell A. *Acta Materialia*[J], 2007, 55(13): 4419
- Wen Y H, Simmons J P, Shen C C et al. *Acta Materialia*[J], 2003, 51(4): 1123
- Wang Y, Banerjee D, Su C C et al. *Acta Materialia*[J], 1998, 46(9): 2983
- Boisse J, Lecoq N, Patte R et al. *Acta Materialia*[J], 2007, 55(18): 6151
- Mushongera L T, Fleck M, Kundin J et al. *Advanced Engineering Materials*[J], 2015, 17(8): 1149
- Yang M, Wei H, Zhang J et al. *Computational Materials Science*[J], 2017, 129: 211
- Elder K, Gould H, Tobochnik J. *Computers in Physics*[J], 1993, 7(1): 27
- Zhou N, Shen C, Wagner M et al. *Acta Materialia*[J], 2010, 58(20): 6685
- John W C, Hilliard J E. *The Journal of Chemical Physics*[J], 1958, 28(2): 258
- Wang Y, Khachaturyan A G. *Acta Metallurgica Et Materialia*[J], 1995, 43(5): 1837
- Wang Y, Chen L Q, Khachaturyan A G. *Scripta Metallurgica et Materialia*[J], 1991, 25(6): 1387
- Xu W W, Han J J, Wang Z W et al. *Intermetallics*[J], 2013, 32: 303
- Lifshitz I M, Slyozov V V. *Journal of Physics & Chemistry of Solids*[J], 1961, 19(1): 35
- Li H Y, Zuo L L, Song X P et al. *Rare Metals*[J], 2009, 28(2): 197

- 26 Molen E H V D, Oblak J, Krieger O H. *Metallurgical Transactions*[J], 1971, 2(6): 1627
- 27 Wang Y B, Peng L M, Wu Y J et al. *Computational Materials Science*[J], 2015, 100: 166

## Co-Ti 合金中 $\gamma$ 相粗化动力学的实验研究和相场模拟

王翠萍<sup>1</sup>, 黄剑洪<sup>1</sup>, 卢 勇<sup>1</sup>, 刘兴军<sup>1,2</sup>

(1. 厦门大学 福建省材料基因工程重点实验室, 福建 厦门 361005)

(2. 哈尔滨工业大学深圳研究院, 广东 深圳 518055)

**摘 要:** 本研究结合实验和相场法研究了反相 Co-19.7Ti 合金中无序  $\gamma$  析出相的组织演变和粗化行为。实验和模拟结果皆表明  $\gamma$  相的形貌随时效时间增加由近球形转变成条状。 $\gamma$  相平均粒径的粗化动力学遵循  $r^3=kt$ , 可获得如下  $\bar{r}_t^3 = 1.126 \times 10^{19} t \exp[-349890/RT]$ 。 $\gamma$  相平均粒径随时效时间的变化分为两个阶段, 阶段 I 增长快速而阶段 II 增长速度减缓。时效温度由 700 °C 增至 750 °C,  $\gamma$  相粒径分布的峰值变大以及粒径分布的宽度变窄, 模拟结果与实验结果取得良好的一致性。

**关键词:** Co-19.7Ti合金; 相场法; 粗化动力学; 温度

---

作者简介: 王翠萍, 女, 1963 年生, 博士, 教授, 厦门大学材料学院, 福建 厦门 361005, 电话: 0592-21878882, E-mail: wangcp@xmu.edu.cn